

Differential Flow of Protons in $Au + Au$ Collisions at AGS Energies

P. K. Sahu¹ and W. Cassing²

¹Institute of Physics, Bhubaneswar 751005, India

²Institut für Theoretische Physik, Universität Giessen
D-35392 Giessen, Germany

November 13, 2018

Abstract

We study the proton sideward and elliptic differential flow for $Au + Au$ collisions at AGS energies (2 – 8 A·GeV) in a microscopic relativistic transport model that includes all baryon resonances up to a mass of 2 GeV as well as string degrees of freedom for the higher hadronic excitations. In order to explore the sensitivity of the various differential flows to the nuclear equation of state (EoS) we use three different parameterizations of the scalar- and vector mean-fields, i.e. NL2 (soft), NL23 (medium) and NL3 (hard), with their momentum dependence fitted to the experimental Schrödinger equivalent potential (at normal nuclear matter density ρ_0) up to kinetic energies of 1 GeV. We calculate the excitation function of sideward and elliptic flow within these parameter sets for $Au + Au$ collisions and compare with the recent data from the E895 Collaboration as a function of rapidity, impact parameter and transverse momentum, respectively. We find that the best description of the differential data is provided by a rather 'stiff' EoS at 2 A·GeV (NL3) while at higher bombarding energies (4–8 A·GeV) a 'medium' EoS leads to the lowest χ^2 with respect to the data. However, the differences in the transverse and elliptic flows (from the different parameter sets) become of minor significance at 4–8 A·GeV. We attribute this insensitivity to a similar reduction of the vector potential in all models and to the dominance of string degrees of freedom at these bombarding energies.

PACS: 25.75.+r, 24.10.Jv

Keywords: Relativistic heavy-ion collisions, relativistic models, collective flow

1 Introduction

According to lattice calculations of QCD a phase transition from an interacting hadronic matter to partonic matter (interacting quarks and gluons) is expected at temperatures $T_c \approx 150 - 180$ MeV for vanishing quark chemical potential [1]. Recent extrapolations to finite quark chemical potentials $\mu_q \neq 0$ suggest a decrease of the critical temperature T_c with increasing μ_q [2]. Whereas rather low chemical potentials (~ 30 MeV) can be probed in central $Au + Au$ collisions at the full RHIC energy ($\sqrt{s} = 200$ GeV) [3, 4], sizeable chemical potentials or baryon densities are encountered in nucleus-nucleus collisions at AGS energies of 2–11 A·GeV. Currently one expects the phase transition at low μ_q to be of second order [5, 6] and a tricritical point for $\mu_q \approx 230$ MeV, $T_c(\mu_q) \approx 160$ MeV [7]. Such conditions might be encountered in $Au + Au$ collisions at AGS energies leading eventually to a softening of the hadronic equation of state (EoS) since the pressure in the partonic phase is expected to be lower than in the hadronic regime. A decrease of the pressure, furthermore, should go along with a decrease of the collective flow of hadrons once the phase boundary is met [8]. Thus a systematic study of flow variables in energetic nucleus-nucleus collisions might indicate the appearance of a new phase of hadronic matter [9]. We recall, that the collective flow observable has been exploited for more than a decade to obtain information on the EoS [10] - [33].

In the last years both, the directed transverse flow (sideward flow) and the flow tensor (elliptic flow), have been measured [9, 16, 20, 21, 22, 34, 35] for heavy-ion ($Au + Au$) collisions at AGS energies in the incident energy range of $2 \text{ A}\cdot\text{GeV} \leq E_{inc} \leq 11 \text{ A}\cdot\text{GeV}$. More recently, also differential flow data have become available from the E985 Collaboration [36] which allow for more severe constraints on the EoS.

The sideward flow is produced at the early stage of nucleus-nucleus collisions and hence reflects the early pressure gradients in the collisions. Thus the strength of the momentum per particle $\langle p_x \rangle (y)$ in the reaction plane versus rapidity y sheds some light on the initial pressure since the gradients are dominated by the collision geometry. The elliptic flow emerges from the early squeeze-out of compressed matter that - depending on bombarding energy - is shadowed by the spectator nucleons. At low energies this squeeze-out of nuclear matter leads to a negative elliptic flow since projectile and target spectators distort the collective expansion of the 'fireball' in the reaction plane. At high energies the projectile and target spectators do not hinder anymore the in-plane expansion of the 'fireball' due to their high velocity ($\approx c$); the elliptic flow then becomes positive. The competition between squeeze-out and in-plane elliptic flow at AGS energies depends on the nature of the nuclear force as pointed out by Danielewicz et al. [18]. Furthermore, it has been suggested in Ref. [36] that the elliptic flow is sensitive to the stiffness of the EoS and possibly to quark-gluon plasma (QGP) formation.

In Refs. [37, 38, 39] both the sideward and elliptic flow of nucleons has been studied for various nucleus-nucleus collisions as a function of beam energy from 0.05 A·GeV [39] to 11 A·GeV [38] employing a relativistic transport model with hadronic and string degrees of freedom. In the AGS energy regime, however, our calculations

have been performed only with a 'stiff' EoS based on momentum-dependent scalar and vector self energies for the nucleons. Here we continue our studies within the same transport approach using, furthermore, different equations of state with incompressibilities of 210 MeV (soft), 300 MeV (medium), and 380 MeV (hard). Moreover, we will confront our calculations with the recent differential flow data from the E985 Collaboration [36] as a function of impact parameter, rapidity and transverse momentum.

We organize our work as follows: In Section 2 we briefly describe the relativistic transport approach and fix the parameter sets for the scalar and vector self energies in comparison to the 'experimental' optical potential from Ref. [40]. In Section 3 we will systematically study the transverse in-plane flow for $Au + Au$ collisions from 2–8 A-GeV while Section 4 concentrates on elliptic flow as a function of impact parameter or momentum, respectively. Section 5 concludes this study with a summary and discussion of open questions.

2 Description of the transport approach

Our studies are based on the relativistic hadron-string model used in Ref. [38] for the investigation of transverse and elliptic baryon flow at AGS energies. The approach is based on a coupled set of covariant transport equations for the phase-space distributions of hadrons which involve the propagation in momentum-dependent scalar and vector mean fields as well as transition rates for elastic and inelastic scattering processes. In the collision terms we employ the in-medium cross sections as given in Ref. [41], that are parameterized in line with the corresponding experimental data (in vacuum) for $\sqrt{s} \leq 3.5$ GeV, while for higher invariant energies \sqrt{s} the Lund string formation and fragmentation model [42] is employed as in the Hadron-String-Dynamics (HSD) approach [43, 44], which has been used extensively for the description of particle production in nucleus-nucleus collisions from SIS to SPS energies [43]. We note, that the 'string threshold' of 3.5 GeV has been determined by a fit to the transverse mass spectra of protons in central $Au + Au$ collisions at AGS energies (cf. Ref. [38]).

The mean-field part of the relativistic transport model is fully specified by the scalar and vector potentials, which determine the mean-field propagation of the hadrons. Once these potentials are specified, the energy per particle E/A as a function of density ρ (EoS) can be calculated for nuclear matter ground-state configurations in a straight forward manner [24, 45]. We recall that in a simple relativistic mean-field theory one assumes the scalar and vector fields to be represented by point-like meson-baryon (i.e. momentum independent) couplings. Such models explain the Schrödinger-equivalent potential (nucleon optical potential) at low kinetic energies ($E_{kin} \leq 200$ MeV) in nuclear matter also in accordance with data [40] and more sophisticated Dirac-Brueckner calculations [46, 47, 48]. However, at higher kinetic energies ($200 \text{ MeV} \leq E_{kin} \leq 1$ GeV), this local relativistic mean-field theory does no longer describe the nucleon optical potential - as extracted from

elastic $p + A$ scattering [40] - due to its linear function in E_{kin} . Since the energy dependence of sideward flow and elliptic flow are controlled in part by the nucleon optical potential, a local relativistic mean-field model cannot be applied anymore to high-energy heavy-ion collisions [37]. In order to take care of this aspect we invoke an explicit momentum-dependence of the coupling constants, i.e. a form factor for the meson-baryon couplings [43, 44] as also used in [38].

In the present calculations we consider Lagrangian densities with nucleon, σ (scalar) and ω (vector) fields and nonlinear self-interactions of the scalar field as in [38], however, with different parameter sets. These parameter sets are denoted by NL2 (incompressibility $K=210$ MeV, soft), NL23 ($K=300$ MeV, medium) and NL3 ($K=380$ MeV, hard) according to the stiffness of the EoS, respectively[26, 45]. For all these parameter sets scalar and vector form factors at the vertices are introduced in the form [38]

$$f_s(\mathbf{p}) = \frac{\Lambda_s^2 - a\mathbf{p}^2}{\Lambda_s^2 + \mathbf{p}^2} \quad \text{and} \quad f_v(\mathbf{p}) = \frac{\Lambda_v^2 - b\mathbf{p}^2}{\Lambda_v^2 + \mathbf{p}^2}. \quad (1)$$

In (1) the cut-off parameters Λ_s and Λ_v and constants a and b are obtained by fitting the Schrödinger equivalent potential,

$$U_{sep}(E_{kin}) = U_s + U_0 + \frac{1}{2M}(U_s^2 - U_0^2) + \frac{U_0}{M}E_{kin}, \quad (2)$$

to Dirac phenomenology for intermediate energy proton-nucleus scattering [40]. These parameters Λ_s , Λ_v , a and b are 1.05 GeV, 1.52 GeV, 1/3 and 1/4 for NL2, 1.0 GeV, 1.35 GeV, 1/3 and 1/4 for NL23 and 1.0 GeV, 0.9 GeV, 1/2 and 1/6 for NL3, respectively. The above momentum dependence is computed self-consistently on the mean-field level as in Ref. [38].

Fig. 1 displays the resulting Schrödinger equivalent potential (2) at density $\rho_0 = 0.168 \text{ fm}^{-3}$ as a function of the nucleon kinetic energy E_{kin} with respect to the nuclear matter at rest for all three models NL2 (solid line), NL23 (dotted line) and NL3 (dot-dashed line). These models are compared with the data from Hama et al. [40] (full squares) which are well described due to the explicit fit. Since the data are only available up to 1 GeV our extrapolations via (1) to higher kinetic energies have to be taken with care. However, as shown in Refs. [37, 38] a decrease of U_{sep} with energy is necessary to properly describe the transverse flow of nucleons in heavy-ion reactions at AGS energies. We mention, that the form factors (1) lead to negative optical potentials for high energies which we consider as unphysical; for simplicity we have set the potentials to zero above 3.2 GeV, 2.8 GeV and 3.5 GeV for NL2 (solid line), NL23 (dashed line) and NL3 (dot-dashed line), respectively, as illustrated in Fig. 1.

It is interesting to note that in order to match the Schrödinger equivalent potentials up to 1 GeV kinetic energy, the strength of the vector potential (with a momentum-dependent form factor) for the soft equation of state (NL2) is higher than for the stiffer equations of state (NL23 and NL3). Since the vector potentials

must be partly compensated by the attractive scalar potentials according to (2) this also holds true for the strength of the scalar potentials.

The energy per nucleon E/A - as resulting from the 3 parameter sets - is shown in the upper left part of Fig. 2 as a function of the density ρ , where the free nucleon mass has been subtracted. The shorthand notations 'soft', 'medium' and 'stiff' become obvious from this figure. It is of further importance, how the optical potentials look like as a function of the baryon momentum p with respect to the nuclear matter at rest e.g. for densities of $2 \rho_0$, $3 \rho_0$, and $5 \rho_0$ which are encountered in nucleus-nucleus collisions at AGS energies. This information is also displayed in Fig. 2 for NL2 (solid lines), NL23 (dotted lines) and NL3 (dot-dashed lines). Whereas for low momentum p the optical potential U_{sep} becomes more repulsive with increasing stiffness K (and density ρ), it is of roughly the same size at all densities for $p \approx 1$ GeV/c and even most repulsive for the 'soft' parameter set NL2 above ~ 1.5 GeV/c. Thus the energy per particle E/A in the upper left part of Fig. 2 is somewhat misleading since it only reflects the momentum dependence of the potentials up to the Fermi momentum

$$p_F = \left(\frac{3}{2}\pi^2\rho\right)^{1/3}, \quad (3)$$

which is less than 0.5 GeV/c even at $6 \rho_0$.

Some further note of caution has to be added here concerning the interpretation of 'baryons per volume', i.e. the density ρ , since in the transport model the initial high density phase is described not by 'formed' baryons but by 'strings', that correspond to continuum excitations of the hadrons. Thus, when addressing the baryon density, we actually consider the constituent quark number per volume - as contained in the strings - and divide by 3 in order to define the baryon density ρ . As shown explicitly in Fig. 11 of Ref. [49] for central $Au + Au$ reactions at 11.6 GeV/c, the initial high density phase of the reaction is fully dominated by quarks and diquarks that form the endpoints of the strings. In this respect we compute the quark current $j_\mu(t, \mathbf{r})$ and define the 'baryon' density as

$$\rho(t, \mathbf{r}) = \rho(x) = \frac{1}{3}\sqrt{j_\mu(x)j^\mu(x)}. \quad (4)$$

3 Transverse flow

In this Section we restrict ourselves to the transverse in-plane flow $\langle p_x \rangle (y)$ for mid-peripheral $Au + Au$ collisions from 2–8 A·GeV. Since the 'input' of the transport approach has been presented in the previous Section we can directly step on with the numerical results in comparison to the experimental data available.

In Fig. 3 we display the average proton in-plane momentum $\langle p_x \rangle (y')$ as a function of the normalized rapidity

$$y' = \frac{y_{cm}}{y_{proj}} \quad (5)$$

for $Au + Au$ systems at 2–8 A·GeV for the impact parameter $b = 6$ fm. Since experimentally the sideward flow is observed for mid-peripheral collisions with an average impact parameter of $b = 6$ fm, we restrict to a single impact parameter here. Note, that the flow only marginally changes with b for mid-peripheral reactions. The solid lines in Fig. 3 correspond to the parameter set NL2 (soft), the dashed lines represent the set NL23 (medium) and the dot-dashed lines the set NL3 (hard). The full squares are the experimental data from the E895 Collaboration [9]. The direct measurements have been performed for $0 \leq y' \leq 1$ and the data for $-1 \leq y' \leq 0$ have been generated by reflection around $y' = 0$. We observe that the overall description of the data is reasonably good for all parameter sets. To quantify the 'agreement' we have performed a χ^2 analysis (for $-0.6 \leq y' \leq 0.6$) and find that the best description is given by the NL3 model at 2 A·GeV, while from 4–8 A·GeV the 'medium' NL23 parameter set performs best. One might interpret this as an indication for a 'softening' of the EoS at ~ 4 A·GeV, however, the differences in the χ^2 values are only small such that this trend has to be interpreted with care.

The shape of $\langle p_x(y') \rangle$ is, furthermore, fitted by a polynomial function

$$\langle p_x(y') \rangle \approx Fy' + Ky'^3 \quad (6)$$

over a finite interval centered around midrapidity. The linear coefficient F in (6) is denoted as sideward flow F . This quantity is shown in Fig. 4 for the parameter sets NL2 (solid line), NL23 (dotted line) and NL3 (dot-dashed line) in comparison to the data from Ref. [9] (full squares). We find that all parameter sets are roughly compatible with the data such that the transverse flow observable F does not qualify very much for a determination of the stiffness of the EoS as pointed out in Ref. [10] more than a decade ago. Only at 2 A·GeV the data more clearly favor a 'stiff' EoS as provided by NL3. The reasonable description of the transverse flow F at 4–8 A·GeV by all parameter sets is attributed to the fact that the momentum and density dependence of the scalar and vector mean fields is roughly the same for momenta $p \geq 0.5$ GeV/c (cf. Figs. 1 and 2), which is enforced by the fit to the experimental data from Hama et al. [40].

The significant decrease in F for bombarding energies above 2 A·GeV is due to the reduction of the vector potentials with momentum as pointed out before in Ref. [38]. According to our understanding the reduction of the vector coupling with density and momentum is a genuine phenomenon of nuclear many-body physics and points towards a restoration of chiral symmetry with increasing density as advocated by Brown and Rho [51]; it not necessarily has to be interpreted as a signature for a phase transition to a QGP.

4 Elliptic flow

We now turn to the results of our calculations for the elliptic flow $v_2(b, p_t)$. The elliptic flow can be measured by the second Fourier coefficient of the azimuthal

distribution of particles with respect to the reaction plane and is characterized by the expectation value [50],

$$v_2 = \langle (p_x^2 - p_y^2) / (p_x^2 + p_y^2) \rangle. \quad (7)$$

In Fig. 5 we show the impact parameter b dependence of the elliptic flow (7) for $Au + Au$ collisions at energies of 2, 4 and 6 A·GeV without any cut on the transverse momentum p_t of the protons. As before, the solid lines display the results from the set NL2, the dotted lines those from NL23 and the dot-dashed lines those from NL3. The experimental data (full squares) have been taken from Ref. [36]. We note that the impact parameter determination from experiment only holds within ± 1 fm. At 2 A·GeV we observe a clear sensitivity to the stiffness of the EoS; only the set NL3 (stiff) describes the large negative elliptic flow as a function of b correctly, whereas the other parameter sets turn out too low in v_2 . This finding agrees with that from Danielewicz [18] that the 2 A·GeV data for $Au + Au$ 'need' a stiff EoS. However, contrary to Ref. [18] we do not find convincing indications for a softening of the EoS at higher bombarding energy. The χ^2 fits to the data in Fig. 5 give only a tiny preference to the results from NL23 (medium) at 6 A·GeV, whereas NL3 (stiff) and NL23 (medium) practically have the same χ^2 at 4 A·GeV.

The situation might change when looking at the elliptic flow at high transverse momentum p_t . We thus compare in Fig. 6 our calculations on the elliptic flow as a function of impact parameter b with the respective data from Ref. [36] for a cut in $p_t \geq 0.7$ GeV/c for $Au + Au$ at 2 and 4 A·GeV. Again clearly the best description at 2 A·GeV is given by NL3 (stiff) now even slightly underestimating the magnitude of v_2 . On the other hand, our results for the soft EoS (given by NL2) give the wrong sign of v_2 at 4 A·GeV which in the experiment is small, but negative at high p_t . At 4 A·GeV the best χ^2 is provided by NL23 (medium), but the sign of v_2 comes out wrong for $6 \text{ fm} \leq b \leq 8 \text{ fm}$, where the elliptic flow is described best by NL3 (stiff). We thus do not find a convincing indication for a softening of the EoS at 4A·GeV.

We continue with a comparison of our calculations to the data from [36] for the elliptic flow at 6 A·GeV imposing a high p_t cut of 1 GeV/c in Fig. 7. Within experimental error bars now all parameter sets show results that are compatible with the data. A χ^2 analysis gives a slight preference for NL23 (medium) followed by NL2 (soft), whereas the χ^2 is higher for NL3 (stiff). However, these differences are still within the statistical accuracy of the transport calculations which becomes poor for high transverse momentum protons. We attribute this approximate insensitivity to the stiffness of the EoS to the fact, that the optical potentials at high density and momenta $p \geq 0.5$ GeV are roughly the same (cf. Fig. 2) and that multi-meson production channels from string decays start to dominate the reaction dynamics above 4 A·GeV as pointed out before in Ref. [38].

5 Summary and Discussion

In summary, we have analyzed the sideward and elliptic flow from $Au + Au$ collisions at beam energies from 2 A·GeV to 8 A·GeV at AGS energies using different nuclear forces that involve 'soft', 'medium' and 'stiff' equation of states in the microscopic relativistic transport model.

The measured sideward flow or the average in-plane momentum as a function of rapidity can be described in the dynamical transport model by practically all parameter sets thus demonstrating that the transverse flow is rather insensitive to the stiffness of the EoS, but crucially depends on the momentum dependence of the mean fields [10]. The rather good description of the transverse flow F by all parameter sets in turn is attributed to the fact that the momentum dependence of the scalar and vector mean fields is roughly the same (cf. Figs. 1 and 2), which is enforced by the fit to the experimental data from Hama et al. [40]. A χ^2 analysis here favors a 'stiff' EoS at 2 A·GeV while the 4-8 A·GeV data are best reproduced by the 'medium' parameter set NL23. However, the significance for this trend is very low.

Our calculations for the elliptic flow v_2 (7) show a clear sensitivity to the stiffness of the EoS at 2 A·GeV; only the set NL3 (stiff) describes the large negative elliptic flow seen by E895 [36] as a function of b correctly, whereas the other parameter sets turn out too low. This finding agrees with that from Danielewicz [18] that the 2 A·GeV data for $Au + Au$ call for a stiff EoS. However, contrary to Ref. [18] we do not find convincing indications for a softening of the EoS at higher bombarding energy even when gating on high transverse momenta ($p_t \geq 0.7$ GeV/c or 1 GeV/c, respectively). A χ^2 analysis favors again the 'medium' EoS (given by the set NL23) at 4-6 A·GeV in line with the analysis of the transverse flow, but with rather low significance. For bombarding energies ≥ 6 A·GeV our calculations turn out to be almost insensitive to the stiffness of the EoS, which is likely due to the fact that the optical potentials at high density and momenta $p \geq 0.5$ GeV (in the transport approach) are roughly the same (cf. Fig. 2) and that multi-meson production channels from string decays start to dominate the reaction dynamics above 4 A·GeV [38].

The open questions – and uncertainties in the transport approach – are related to the explicit momentum dependence of the optical potential U_{sep} (2) in the kinematical range above 1 GeV of relative kinetic energy. Here data from elastic proton-nucleus scattering at AGS would be of significant help to pin down the present uncertainties. Furthermore, the question of the 'effective degrees of freedom' encountered in the early phase of nucleus-nucleus collisions at AGS energies is open, too. The fact, that our transport calculations – involving all hadrons up to a mass of 2 GeV and strings for the hadronic continuum – give a good description of the differential sideward and elliptic flow data, does not imply that the proper degrees of freedom are employed. On the other hand, we can turn the argument around and conclude, that the differential flow data do not necessarily indicate the presence of a new state of matter such as the QGP. Electromagnetic signals (hard photons,

dileptons or 'penetrating' probes) should provide complementary information to the collective observables studied here. Unfortunately, such information is not available from the AGS; related studies are foreseen at the future GSI upgrade [52].

References

- [1] F. Karsch and E. Laermann, Phys. Rev. D **50** (1994) 6954.
- [2] C. R. Allton et al., hep-lat/0204010.
- [3] P. Braun-Munzinger et al., Phys. Lett. B **518** (2000) 41.
- [4] I. G. Bearden et al., nucl-ex/0207006.
- [5] M. Stephanov, K. Rajagopal and E. Shuryak, Phys. Rev. Lett. **81** (1998) 4816.
- [6] E. V. Shuryak, Nucl. Phys. A **661** (1999) 119c.
- [7] Z. Fodor and S. D. Katz, Phys. Lett. B **534** (2002) 87; JHEP **0203** (2002) 014.
- [8] D. Rischke, Nucl. Phys. A **610** (1996) 88c.
- [9] E895 Collaboration, H. Liu et al., Phys. Rev. Lett. **84** (2000) 5488.
- [10] W. Cassing and U. Mosel, Prog. Part. Nucl. Phys. **25** (1990) 235.
- [11] H. Stöcker and W. Greiner, Phys. Rep. **137** (1986) 277.
- [12] H. H. Gutbrod, A. M. Poskanzer and H. G. Ritter, Rep. Prog. Phys. **52** (1989) 1267.
- [13] C. Gale, G. M. Welke, M. Prakash, S. J. Lee, and S. Das Gupta, Phys. Rev. C **41** (1990) 1545.
- [14] J. Zhang, S. Das Gupta and C. Gale, Phys. Rev. C **50** (1994) 1617.
- [15] M. D. Partlan et al., Phys. Rev. Lett. **75** (1995) 2100.
- [16] N. Herrmann et al., Nucl. Phys. A **610** (1996) 49c.
- [17] J. Chance et al., Phys. Rev. Lett. **78** (1997) 2535.
- [18] P. Danielewicz et al., Phys. Rev. Lett. **81** (1998) 2438; P. Danielewicz, Nucl. Phys. A **673** (2000) 34; P. Danielewicz, Nucl. Phys. A **685** (2001) 368.
- [19] J. -Y. Ollitrault, Phys. Rev. D **46** (1992) 229; H. Sorge, Phys. Rev. Lett. **78** (1997) 2309.
- [20] W. Reisdorf and H. G. Ritter, Ann. Rev. Nucl. Part. Sci. **47** (1997) 1.
- [21] P. Braun-Munzinger and J. Stachel, Nucl. Phys. A **638** (1998) 3c.
- [22] P. Chung et al., J. Phys. G **25** (1999) 255.
- [23] Q. Pan and P. Danielewicz, Phys. Rev. Lett. **70** (1993) 2062.
- [24] T. Maruyama, W. Cassing, U. Mosel, S. Teis and K. Weber, Nucl. Phys. A **573** (1994) 653.

- [25] S.A. Bass et al., Prog. Part. Nucl. Phys. **41** (1998) 225 ; J. Phys. **G 25** (1999) R1.
- [26] S. K. Ghosh, S. C. Phatak and P. K. Sahu, Z. Phys. **A352** (1996) 457.
- [27] B.-A. Li, C. M. Ko, A. C. Sustich, and B. Zhang, Phys. Rev. **C 60** (1999) 011901.
- [28] J. Brachmann et al., Phys. Rev. **C 61** (2000) 024909.
- [29] Y. Nara, N. Otuka, A. Ohnishi, K. Niita and S. Chiba, Phys. Rev. **C 61** (2000) 024901.
- [30] A.Hombach, W. Cassing, S. Teis and U. Mosel, Eur. Phys. J. **A 5** (1999) 157.
- [31] Y. Nara, N. Otuka, A. Ohnishi and T. Maruyama, Prog. Theor. Phys. Suppl. **129** (1997) 33.
- [32] M. Belkacem, M. Brandstetter, S. A. Bass et al., Phys. Rev. **C 58** (1998) 1727; L. V. Bravina et al., J. Phys. **G 25** (1999) 351.
- [33] L. V. Bravina, A. Faessler, C. Fuchs, and E. E. Zabrodin, Phys. Rev. **C 61** (2000) 064902.
- [34] E895 Collaboration, P. Chung et al., Phys. Rev. Lett. **86** (2001) 2533.
- [35] E895 Collaboration, J. L. Klay et al., Phys. Rev. Lett. **88** (2002) 102301.
- [36] E895 Collaboration, P. Chung et al., nucl-ex/0112002.
- [37] P. K. Sahu, A. Hombach, W. Cassing, M. Effenberger and U. Mosel, Nucl. Phys. **A 640** (1998) 493.
- [38] P.K. Sahu, W. Cassing, U. Mosel and A. Ohnishi, Nucl. Phys. **A 672** (2000) 376.
- [39] A. B. Larionov, W. Cassing, C. Greiner, and U. Mosel, Phys. Rev. **C 62** (2000) 064611.
- [40] S. Hama, B. C. Clark, E. D. Cooper, H. S. Sherif and R. L. Mercer, Phys. Rev. **C 41** (1990) 2737.
- [41] M. Effenberger, E. L. Bratkovskaya and U. Mosel, Phys. Rev. **C 60** (1999) 044614.
- [42] B. Nilsson-Almqvist and E. Stenlund, Comp. Phys. Comm. **43** (1987) 387; B. Anderson, G. Gustafson and Hong Pi, Z. Phys. **C 57** (1993) 485.
- [43] W. Cassing and E. L. Bratkovskaya, Phys. Rep. **308** (1999) 65.
- [44] W. Ehehalt and W. Cassing, Nucl. Phys. **A 602** (1996) 449; J. Geiss, W. Cassing and C. Greiner, Nucl. Phys. **A 644** (1998) 107.
- [45] A. Lang, B. Blättel, W. Cassing, V. Koch, U. Mosel and K. Weber, Z. Phys. **A 340** (1991) 207.
- [46] W. Botermans and R. Malfliet, Phys. Rep. **198** (1990) 115.

- [47] T. Gross-Boelting, C. Fuchs, and A. Faessler, Nucl. Phys. **A 648** (1999) 105.
- [48] C. Fuchs, D. Waindzoeh, A. Faessler, and D. S. Kosov, Phys. Rev. **C 58** (1998) 2022.
- [49] W. Cassing, Nucl. Phys. **A 700** (2002) 618.
- [50] STAR Collaboration, K. H. Ackermann et al., Phys. Rev. Lett. **86** (2001) 402.
- [51] G. E Brown and M. Rho, Phys. Rep. **363** (2002) 85.
- [52] 'An International Accelerator Facility for Beams of Ions and Antiprotons', <http://www.gsi.de/GSI-Future/cdr/>.

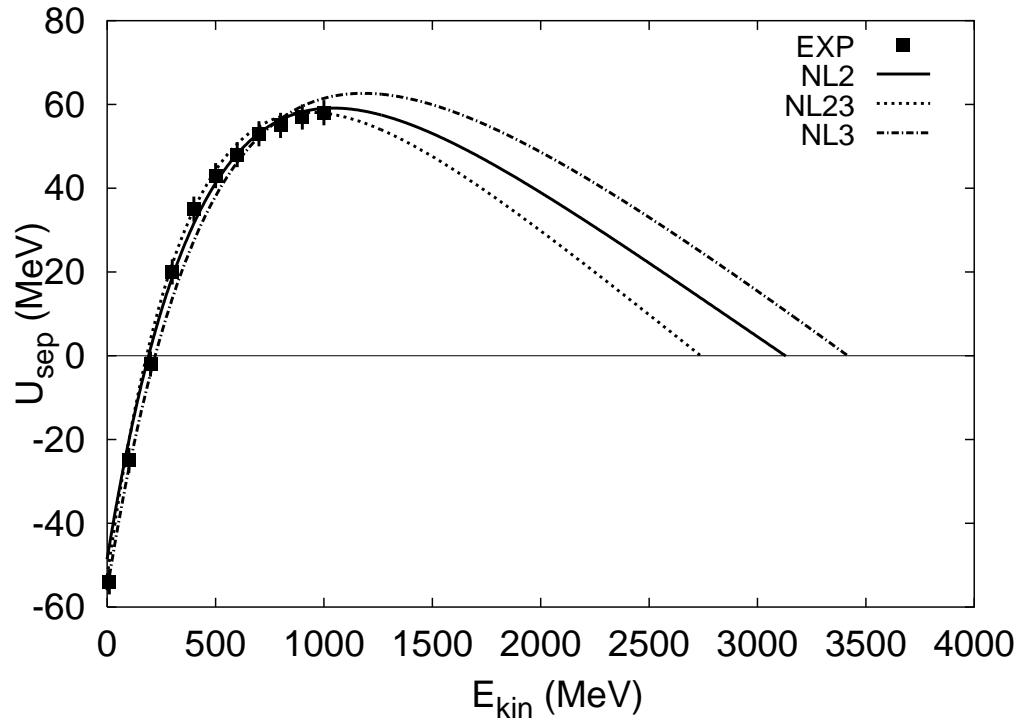


Figure 1: The Schrödinger equivalent potential (2) at density ρ_0 as a function of kinetic energy in comparison to the data are from [40] (full squares). The solid line results from the parameter set NL2 (soft) while the dotted and dot-dashed lines correspond to NL23 (medium) and NL3 (stiff), respectively.

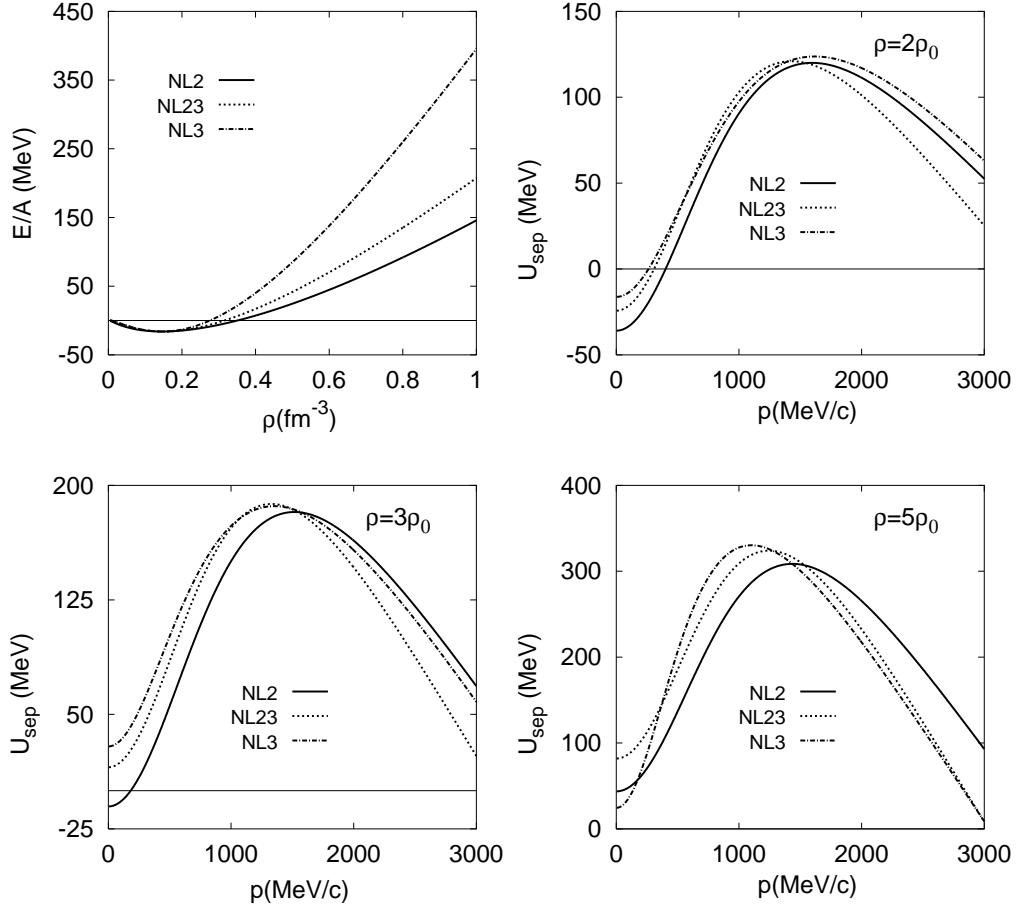


Figure 2: The energy per nucleon E/A as a function of density ρ is shown in the upper left part for the parameter sets NL2 (solid line), NL23 (dotted line) and NL3 (dot-dashed line). The optical potential (2) as a function of the baryon momentum p with respect to the nuclear matter at rest frame is displayed in the upper right and lower parts for densities of $2\rho_0$, $3\rho_0$ and $5\rho_0$, respectively.

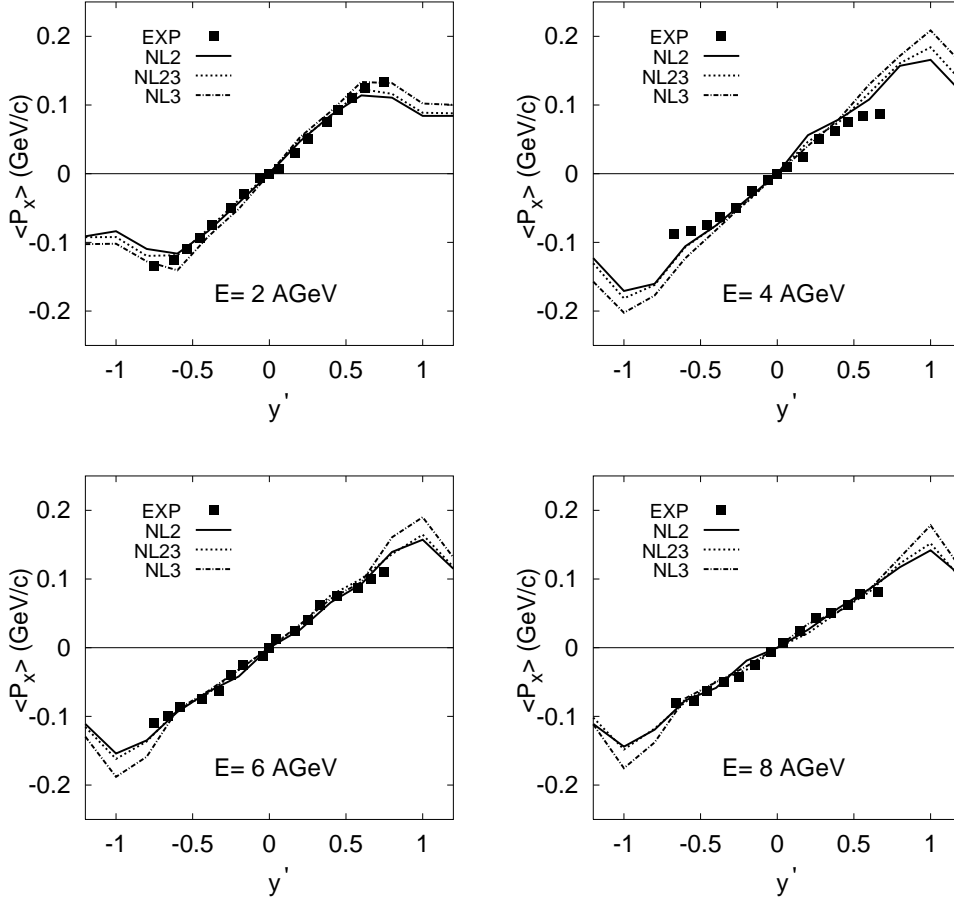


Figure 3: The average proton in-plane momentum as a function of the normalized rapidity y' (5) for $Au + Au$ at 2–8 A·GeV and impact parameter $b = 6$ fm for the parameter sets NL2 (solid lines), NL23 (dotted lines) and NL3 (dot-dashed lines). The experimental data (full squares) are from the E895 Collaboration [9].

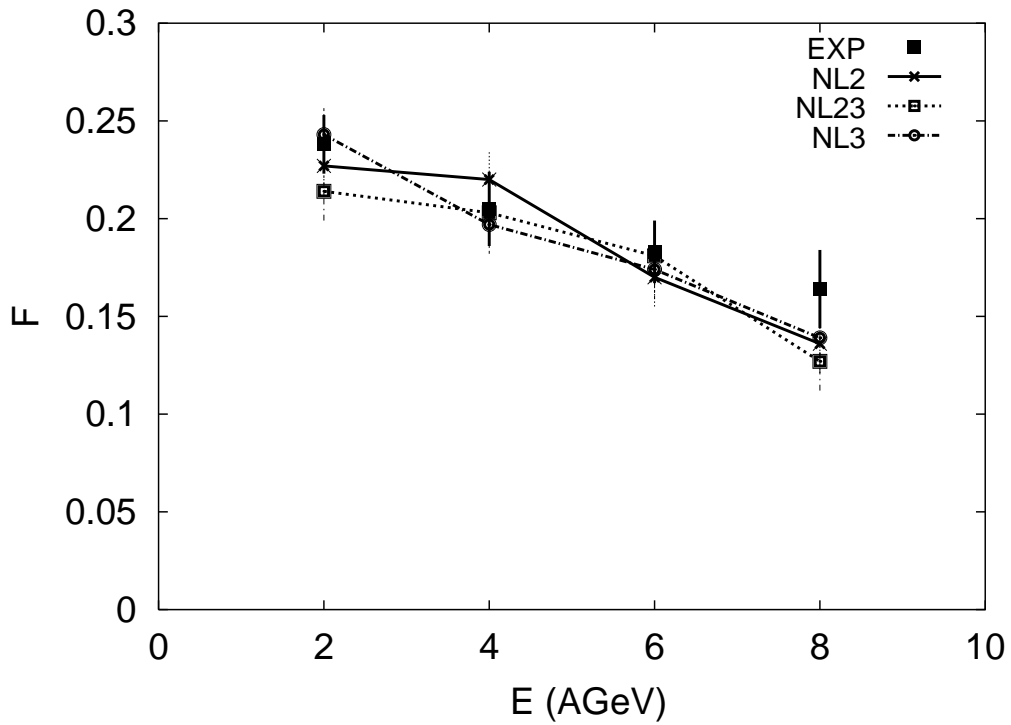


Figure 4: The flow $F(6)$ as a function of beam energy for $Au + Au$ collisions at $b=6$ fm for the parameter sets NL2 (solid line), NL23 (dotted line) and NL3 (dot-dashed line). The experimental data (full squares) are from the E895 collaboration [9].

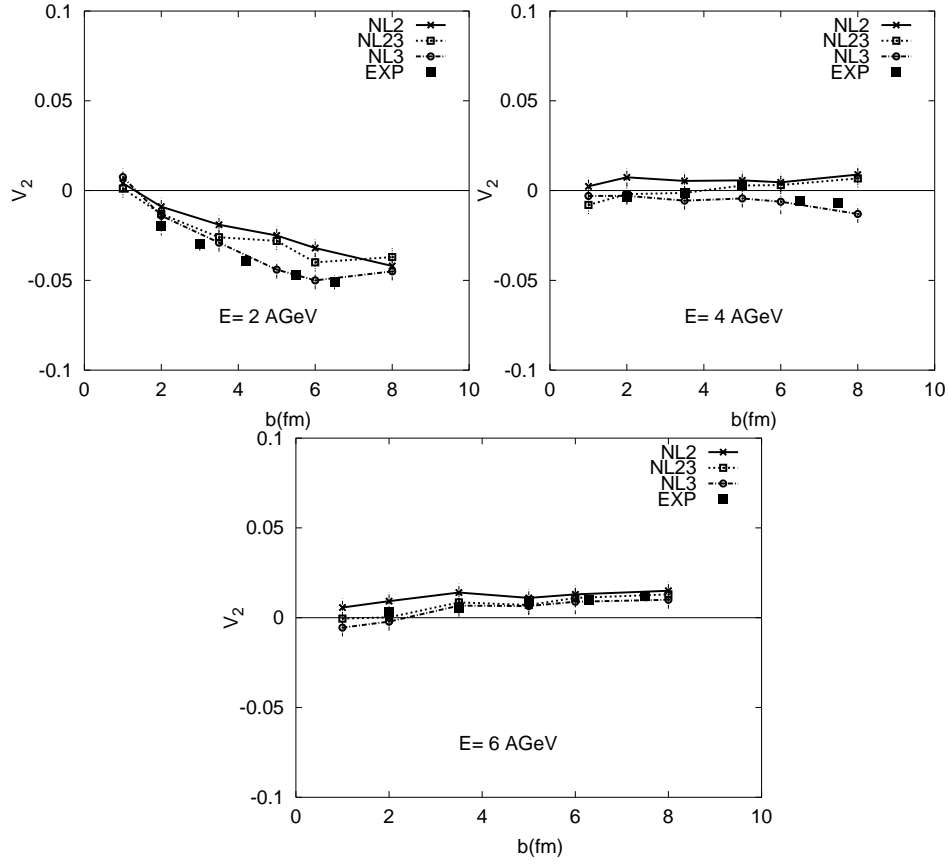


Figure 5: Elliptic flow v_2 (7) as a function of impact parameter b for $Au + Au$ collisions at 2, 4 and 6 A-GeV with $p_t \geq 0$. The experimental data (full squares) are from the E895 Collaboration [36].

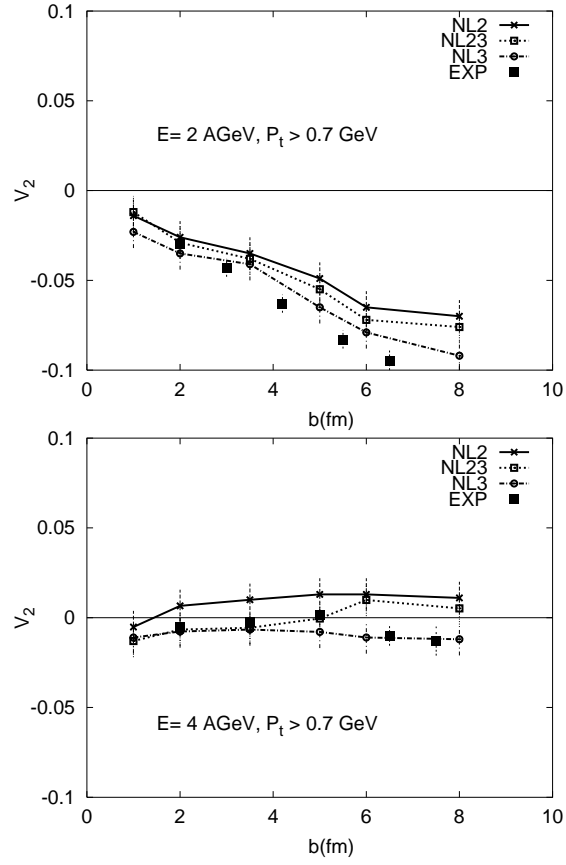


Figure 6: Elliptic flow v_2 (7) as a function of impact parameter b for $Au + Au$ collisions at 2 and 4 A-GeV for $p_t \geq 0.7 \text{ GeV}/c$. The experimental data (full squares) are from the E895 Collaboration [36].

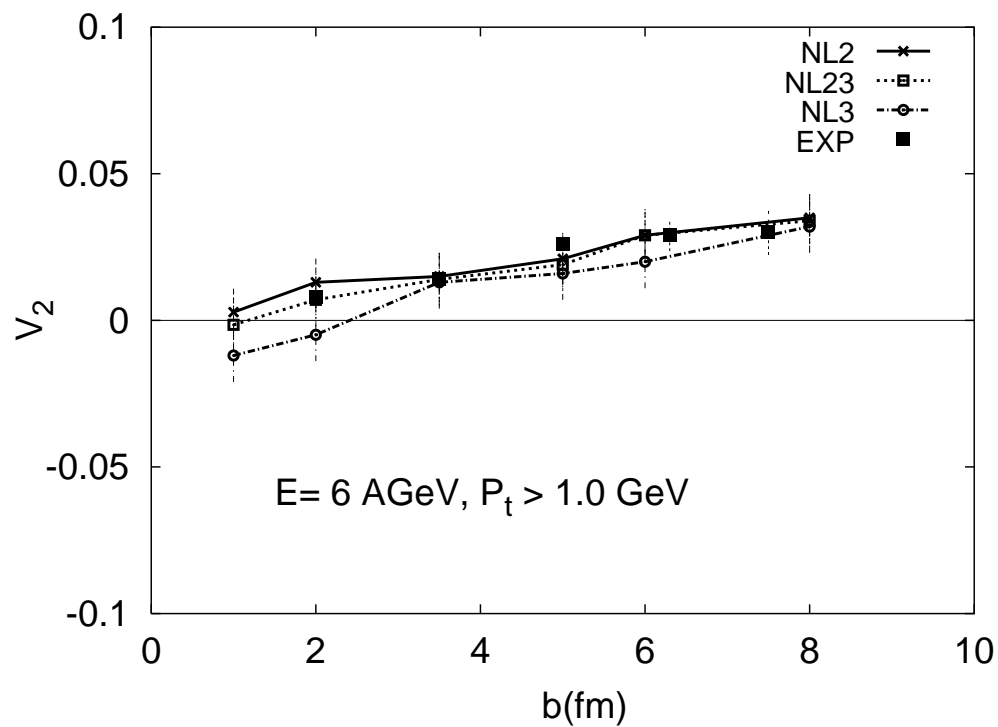


Figure 7: Elliptic flow v_2 (7) as a function of impact parameter b for $Au + Au$ collisions at 6 A·GeV for $p_t \geq 1.0$ GeV/c. The experimental data (full squares) are from the E895 Collaboration [36].